

# Information Sifting Funnel: Privacy-preserving Collaborative Inference Against Model Inversion Attacks

Rongke Liu\*

Nanjing University of Aeronautics and Astronautics  
Nanjing, China  
liurongke@nuaa.edu.cn

## ABSTRACT

The complexity of neural networks and inference tasks, combined with the demand for computational efficiency and real-time feedback, poses significant challenges for resource-constrained edge devices. Collaborative inference addresses this by assigning shallow feature extraction to edge devices and uploading feature to the cloud for subsequent inference, reducing computational pressure. However, transmitted features remain vulnerable to model inversion attacks (MIAs), which can reconstruct original input data. Existing defenses, including perturbation and information bottleneck techniques, provide explainable protection but are limited by the lack of standardized criteria for evaluating MIA difficulty, challenges in mutual information estimation, and trade-offs among usability, privacy, and deployability.

To overcome these limitations, we establish the first criterion for assessing the difficulty of MIAs in collaborative inference, supported by theoretical analysis of existing attacks and defenses and validated through experiments using the Mutual Information Neural Estimator (MINE). Building on these findings, we propose SiftFunnel, a privacy-preserving framework for collaborative inference. Specifically, we first train the edge model with both linear and non-linear correlation constraints to limit redundant information in transmitted features, enhancing privacy protection. Moreover, label smoothing and a cloud-based upsampling module are incorporated to balance usability and privacy. To further support deployability, the edge model is designed with a funnel-shaped structure and integrates attention mechanisms, preserving both privacy and usability. Extensive experiments show that SiftFunnel outperforms state-of-the-art defenses against MIAs, achieving superior privacy protection with less than 3% accuracy loss and an optimal trade-off among usability, privacy, and practicality.

## CCS CONCEPTS

• Security and privacy → Domain-specific security and privacy architectures.

## KEYWORDS

Collaborative inference, model inversion attacks, deep learning security and privacy, information theory

### ACM Reference Format:

Rongke Liu. 2025. Information Sifting Funnel: Privacy-preserving Collaborative Inference Against Model Inversion Attacks. In *Proceedings of ACM Conference on Computer and Communications Security (CCS'25)*. ACM, New York, NY, USA, 15 pages. <https://doi.org/XXXXXXXX.XXXXXXX>

## 1 INTRODUCTION

The rapid advancement of deep learning has produced increasingly complex and powerful neural network models that achieve remarkable performance in tasks like image detection and recognition. However, these advancements also pose significant challenges for edge computing devices [24]. In applications such as intelligent transportation, autonomous driving, facial recognition, IoT applications involving cameras and sensors, and remote healthcare monitoring, edge devices must process data instantly while handling growing computational demands. Their limited resources often make independent execution of complex deep learning inference infeasible [39].

Cloud computing offers substantial computational power for inference by processing data on cloud-based models. However, it faces two major limitations: bandwidth and network latency impede real-time performance, and uploading raw data raises privacy concerns, especially in sensitive scenarios. Collaborative inference (CI) [40] has emerged as a viable solution to these challenges. By partitioning a neural network into  $f_{\text{edge}}$  and  $f_{\text{cloud}}$ , the edge device processes raw inputs into feature representations via  $f_{\text{edge}}$ , which are then transmitted to the cloud for further inference by  $f_{\text{cloud}}$ . This approach balances real-time performance and computational efficiency. CI has been increasingly applied in domains like unmanned aerial vehicles (UAVs) [35], IoT systems [39], and technologies like Apple's private cloud computing (PCC) [11]. With advancements in 5G, IoT, and AI, CI is poised for wider adoption and significant future impact.

However, recent studies have revealed significant privacy risks in collaborative inference, where input data on edge devices can be reconstructed through model inversion attacks (MIAs) [19, 50, 52], as shown in Figure 1. MIAs are fine-grained privacy attacks that leverage the output information of AI models and deep learning generation techniques to reconstruct input data [19, 51], recover representative training data [28, 56], or expose sensitive information [13, 30]. These risks are particularly acute in collaborative inference scenarios, as edge devices, unlike centralized deployments, often rely on shallow neural networks to generate and transmit feature representations. These features, maintaining significantly

Permission to make digital or hard copies of all or part of this work for personal or classroom use is granted without fee provided that copies are not made or distributed for profit or commercial advantage and that copies bear this notice and the full citation on the first page. Copyrights for components of this work owned by others than the author(s) must be honored. Abstracting with credit is permitted. To copy otherwise, or republish, to post on servers or to redistribute to lists, requires prior specific permission and/or a fee. Request permissions from [permissions@acm.org](mailto:permissions@acm.org).  
CCS'25, October 13–17, 2025, xx, xx

© 2025 Copyright held by the owner/author(s). Publication rights licensed to ACM.  
ACM ISBN 978-1-4503-XXXX-X/25/10...\$15.00  
<https://doi.org/XXXXXXXX.XXXXXXX>

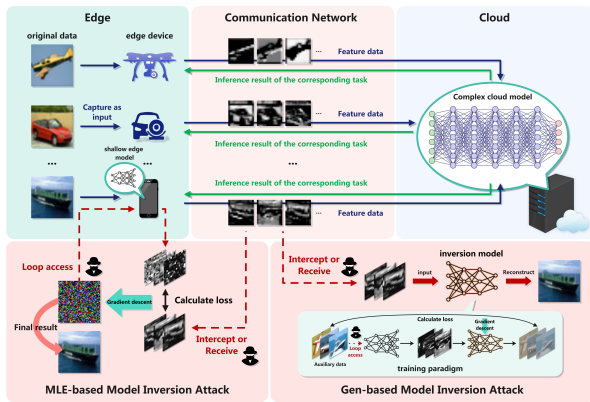


**Figure 1: Collaborative inference and the threat of model inversion attacks.**

higher mutual information with the input data compared to final inference results, render the original inputs susceptible to reconstruction by adversaries [3]. For instance, in facial recognition applications, adversaries in centralized deployments are typically limited to recovering training data through the model API [42, 53]. In contrast, CI enables adversaries to reconstruct raw facial data directly from transmitted features.

The MIA in CI can be divided into two types based on their technical approaches: Maximum Likelihood Estimation-based (MLE-based) MIA [19, 20] and Generative Model-based (Gen-based) MIA [20, 52]. MLE-based MIAs reconstruct input data by iteratively optimizing the input to minimize the loss between the edge model’s output and the transmitted features. While effective for shallow neural networks and low-complexity linear models, this approach relies on the assumption of white-box access to the edge model for gradient-based optimization, significantly limiting its practicality in practical applications. To address these constraints, Gen-based MIAs leverage generative models to approximate the inverse mapping function of the edge model, achieving  $Data \approx Generator(Feature)$ . The success of this method depends on the alignment between the generator’s training data distribution and the edge model’s input data distribution, as well as the generator’s capacity to accurately model the inverse function. The privacy risks posed by MIA have prompted significant research into defense mechanisms, yet challenges remain in analyzing theoretical attacks and balancing usability, privacy preservation, and deployment feasibility.

Firstly, existing defenses in CI are tied to specific technologies while lacking comprehensive theoretical analysis and guidance. We categorize current mainstream defense methods into three types based on their technical approaches: perturbation-based [20, 46], information bottleneck (IB)-based [34, 47], and neural network depth & information bottleneck (NND & IB)-based defense strategies [3, 8]. Perturbation-based strategies enhance defense by introducing perturbations to the gradient for training or trained edge model output information. IB-based strategies focus on approximating the reduction of mutual information  $I(x, z)$  between the input data  $x$  and the feature  $z$ , thus minimizing redundant information about  $x$  in  $z$  [45]. NND & IB-based strategies leverage the observation that increasing the depth of the edge network can induce an information

bottleneck effect, thus enhancing defense. These methods provide theoretically interpretable defense mechanisms, with the introduction of information theory concepts offering notable contributions to defense design. However, existing work lacks a comprehensive understanding of MIA, relies on weak assumptions about adversarial capabilities, and fails to establish a clear criterion for evaluating the difficulty of implementing MIA. As a result, defenses struggle to ensure generalizability against complex attacks and practical scenarios, while addressing future advancements in attack techniques remains challenging.

Secondly, the trade-off between usability, privacy, and deployability in edge models remains a underexplored and challenging area in current research. Encryption-based defense strategies receive limited attention in CI due to resource constraints and the demands of real-time multitask processing [31]. Furthermore, encryption does not guarantee complete data security, as modern side-channel attacks leveraging deep learning can recover encrypted data [22]. The three main defense strategies discussed above also face issues of imbalance. Perturbation-based methods often compromise usability, whereas IB-based defenses aim to reduce  $I(x, z)$ , providing theoretical protection against MLE-based MIA. However, accurately estimating  $I(x, z)$  requires sufficient data and specialized algorithms, limiting its effectiveness against more advanced attacks such as Gen-based MIAs. Adversarial training has been introduced as a component to address the aforementioned issues, but its high specificity and limited interpretability make it difficult to prevent future advanced attacks while significantly increasing the difficulty of training edge models. The NND & IB-based approach aims to balance privacy and usability by increasing model depth, but this comes at the cost of higher resource demands on edge devices, including memory, storage, and bandwidth, thereby reducing deployability. Consequently, such methods are often less favored in practical applications.

Thus, there is a pressing need for a novel approach grounded in an in-depth analysis of attack theories to provide interpretable and effective privacy protection while maintaining the usability and deployability of edge models. This need gives rise to three key technical challenges. *Challenge 1: How to establish an experimentally validated criterion for assessing MIA difficulty in collaborative inference?* Prior studies have interpreted MIA from an information-theoretic perspective, but challenges in computing mutual information and conducting an in-depth analysis of attack principles have hindered the establishment of a verifiable criterion, which is essential for guiding defense design and evaluating methods. *Challenge 2: How to effectively and interpretably remove redundant information from transmitted features while preserving edge model usability?* Although information bottleneck theory provides an interpretable defensive effect, mutual information is challenging to calculate, and current approximation methods are suboptimal. *Challenge 3: How to balance usability and privacy while ensuring practical deployability?* NND & IB-based methods impose significant computational overhead on edge devices, limiting their practicality. Moreover, when applied to edge models designed for simple feature extraction, these methods struggle to counter advanced Gen-based MIAs effectively.

To overcome the aforementioned challenges, we established a criterion  $D_{mia}$  to evaluate the difficulty of MIAs in CI and proposed a lightweight privacy-preserving strategy called Information Sifting

Funnel (SiftFunnel), which incorporates three key characteristics. (1) *SiftFunnel provides interpretable defense principles based on  $D_{mia}$* . We identified factors influencing attack in CI, including  $I(x, z)$ ,  $H(x | z)$ ,  $H(z)$  and the effective information mean  $\delta(z)$ , i.e., the average number of non-zero elements in  $z$ . By analyzing these factors, we clarified defense design directions and developed the SiftFunnel. Using the Mutual Information Neural Estimator (MINE) [4], we quantified the changes in  $I(x, z)$  across different network depths, validating the  $D_{mia}$ . (2) *SiftFunnel effectively reduces redundant information in transmitted features while preserving edge model usability*. Guided by the proposed criterion, the edge model is designed to filter redundant information, focus on task-relevant feature extraction, and ensure usability by integrating Squeeze-and-Excitation (SE) Modules [23], Triple Attention Mechanisms [32], and Convolutional Block Attention Modules (CBAM) [48]. To enhance its resistance to MIAs while maintaining usability, the loss function incorporates Distance-correlation and Pearson-correlation constraints alongside an  $l_1$ -norm constraint on  $z$ . These refinements reduce  $H(z)$ ,  $\delta(z)$  while increasing  $H(x|z)$ . Usability is further preserved through a combination of label-smoothing and KL-divergence loss. (3) *SiftFunnel balances usability and privacy while light-weighting the edge model*. A funnel-shaped edge model is designed to progressively reduce transmitted channels, enhancing efficiency and eliminating redundant information while minimizing memory and storage requirements. To ensure usability, an upsampling module is incorporated on the cloud side.

Based on previous evaluation metrics, we incorporate  $I(x, z)$ , quantified using MINE, and  $\delta(z)$  as metrics to validate theoretical analysis and assess the effectiveness of defense methods. Deployability is assessed through the edge model's parameter count and inference latency. Systematic experiments validate the proposed criterion and demonstrate that SiftFunnel effectively balances usability, deployability, and data privacy compared to existing methods, achieving superior MIA resistance while significantly reducing mutual information and edge model parameters, with only a 3% accuracy trade-off.

Our contributions are summarized as follows.

- We establish the first difficulty criterion for implementing MIA in CI, providing guidance for defense design and laying the foundation for resisting future advanced MIAs.
- We propose SiftFunnel, a privacy-preserving scheme for CI that constrains redundant transmitted features through linear and nonlinear correlation, ensuring model usability with label smoothing and loss function regularization.
- SiftFunnel adopts a funnel-shaped structure with attention blocks to balance usability and privacy while ensuring the lightweight design of edge models.
- We conduct systematic experiments validating the proposed criterion and demonstrating the effectiveness of SiftFunnel in balancing usability, privacy, and deployability.

## 2 BACKGROUND AND RELATED WORK

### 2.1 Collaborative inference

The rapid development of artificial intelligence has enabled deep learning models to achieve exceptional performance in image processing and other tasks. However, the computational demands of

these models often exceed the capabilities of resource-constrained edge devices, which face limitations in processing power, storage, and energy efficiency. To address these challenges, collaborative inference [40] has emerged as an effective solution. This approach divides the inference process into two stages: one part is performed locally on the edge device (which may consist of a single device or a chain of interconnected devices), while the remaining computation is uploaded to the cloud. Formally, this can be expressed as

$$f(x) = f_e(x) \circ f_c(f_e(x)) \quad (1)$$

where  $f$  is the full trained model,  $x$  is the input,  $f_e$  represents the model deployed on the edge, and  $f_c$  corresponds to the portion deployed in the cloud.

Collaborative inference typically begins with training  $f$  on centralized datasets in the cloud, followed by partitioning and deploying the  $f_e$  to the edge. Alternatively, approaches like Split Learning [58] allow edge devices to participate in model training locally. Regardless of the training approach, the inference process remains consistent. As depicted in Figure 1, the edge model computes an intermediate representation, which is transmitted to the cloud for completion of the inference process. The final output is either sent back to the edge device or retained in the cloud for further analysis.

However, existing research [19] highlights that edge models are susceptible to MIAs, where adversaries reconstruct input data from transmitted features. Notably, in edge-based inference, computations can be distributed across multiple devices in a chained architecture [19], expressed as  $f = f_{e1} \circ f_{e2} \dots \circ f_c$ . Studies [20, 21] show that deeper neural networks closer to the cloud transmit more complex, decision-focused features, making them more resistant to reconstruction. In contrast, the initial edge device generates features retaining more input information, making it highly susceptible to MIAs. This paper focuses on the MIA threat to the initial edge device, which employs a shallow neural network while the remaining computation occurs in the cloud. This common scenario in real-world applications presents a significant security risk due to the increased likelihood of input data reconstruction, highlighting the need for effective countermeasures.

### 2.2 Model inversion attack

MIA is a fine-grained privacy attack that uses the output of a target model and adversarial knowledge, such as white-box access or training data distribution, to reconstruct training data [56], sensitive attributes [30], or input data [51]. Initially proposed by Fredrikson et al. [12], MIA was applied to linear regression models, successfully reconstructing genomic data from warfarin dosage predictions and patient attributes, thereby revealing the privacy risks. Subsequent studies [12] extended this concept to deep learning, showing that training data from deep neural networks could also be reconstructed.

Current MIA techniques in CI can be broadly categorized into MLE-based MIAs and Gen-based MIAs, which are further analyzed in the following sections.

**MLE-based MIAs.** MLE-based MIA was first introduced by Fredrikson et al. [12], who reconstructed training data from a multilayer perceptron (MLP) by minimizing the difference between target and confidence scores using gradient descent. Subsequent

research [19] incorporated Total Variation (TV) [37] loss as a regularization term to improve optimization, with these advanced techniques referred to as rMLE-based MIA. In this paper, both are collectively referred to as MLE-based MIA. In CI scenarios, MLE-based methods are particularly effective for reconstructing data from shallow neural networks, as the richer feature representations and lower complexity provide adversaries with detailed gradient information that is easier to optimize compared to the prediction vectors of deeper networks.

**Gen-based MIAs.** This approach was introduced by Yang et al. [51], who reconstructed input data in facial recognition systems by using generative deep learning models  $g$  to approximate the inverse mapping function of the target model  $f^{-1}$ , such that  $g \approx f^{-1}$ . By feeding prediction vectors into  $g$ , they successfully generated facial input images. Building on this approach, He et al. [19] extended it to collaborative inference, demonstrating that input data from edge models is more vulnerable to reconstruction, thereby highlighting the risks. Unlike MLE-based methods, Gen-based MIA does not require white-box access to the edge model. Instead, it trains an attack model by calculating losses based on transmitted features and auxiliary data, enabling it to approximate the inverse mapping of non-linear computations. Furthermore, as edge models produce rich and redundant outputs, this facilitates the training of attack models and the reconstruction process, as analyzed in detail in Section 4.

### 2.3 Related defense work

To safeguard input data collected by edge devices in CI from potential leakage, He et al. [19, 20] emphasized the importance of developing effective defense strategies while identifying these vulnerabilities. Existing defenses can be classified into three main categories: perturbation-based, IB-based, and NND & IB-based approaches. The following sections outline these strategies.

**Perturbation-based defense.** This approach introduces carefully designed noise perturbations into the gradients for training or trained edge model output features to reduce the likelihood of adversaries extracting meaningful information and defend against MIA. He et al. [20] initially proposed using Gaussian noise and random feature dropout to limit the effective information accessible to attackers, and later, Wang et al. [46] extended this strategy by dynamically adjusting the depth of the edge model while adding differential privacy noise to transmitted features. Although these methods enhance defenses, they significantly impact model usability, typically reducing accuracy by approximately 10%, and remain less effective against Gen-based MIA. The root cause is that decoder in Gen-based MIAs is sufficiently expressive to adapt to noise or feature dropout, similar to the training of denoising auto-encoder (DAE) [14], potentially increasing attack robustness. In centralized MIA defenses, Struppek et al. [43] proposed perturbing training labels with a negative label smoothing factor, significantly reducing MIA effectiveness and offering a novel perspective for designing defense strategies.

**IB-based defense.** This approach enhances defenses against inference attacks by limiting the mutual information between input data  $x$  and intermediate features  $z$  while preserving the mutual information between  $z$  and outputs  $y$ , thus maintaining inference

performance [45]. The objective of this defense can be formally expressed as follows:

$$\min_{\theta} -I(z, y) + I(x, z) \quad (2)$$

Initially, Wang et al. [45] introduced information bottleneck theory into MIA defenses, but their method was not optimized for CI and required substantial computational resources for intermediate feature processing. To address this, Peng et al. [34] proposed BiDO (Bilateral Dependency Optimization), which uses dependency algorithms to optimize correlations among inputs, features, and outputs. BiDO reduces input-feature correlation while enhancing feature-output correlation, achieving a balance between defense and performance. Additionally, Wang et al. [47] and Duan et al. [10] explored mutual information estimation between  $x$  and  $z$  using methods based on mutual information definition and the CLUB (Contrastive Log Upper Bound) [5] technique, incorporating the estimates as constraints in training loss function. IB-based defenses provide interpretable protection mechanisms and valuable design insights for future research. However, these methods face limitations: BiDO relies on kernel functions for non-linear correlation constraints, with performance highly sensitive to hyper-parameters like kernel bandwidth; poor parameter selection can lead to suboptimal results. Methods based on mutual information estimation is constrained by sample scale to compute.

**NND & IB-based defense.** Building on the natural advantages of deeper neural networks in resisting attacks and incorporating IB theory, this approach leverages targeted loss functions to enhance defense effectiveness. Expanding on this idea, Ding et al. [8] proposed increasing network depth while compressing newly added hidden layers to restrict redundant information transmission. Subsequently, Azizian et al. [3] further improved defenses by introducing an auto-encoder (AE) structure, with encoders at the edge and decoders at the cloud. The edge encoder increases network depth and reduces feature dimensionality to achieve the IB effect, while the cloud decoder restores information to maintain predictive performance. Additionally, an  $l_1$ -norm constraint is applied during feature transmission to reduce attack risks, and adversarial training is incorporated to strengthen defense robustness against MIAs.

However, this method has certain limitations. First, increasing the depth of neural networks and adding additional modules raises computational and hardware requirements on edge devices, limiting its applicability. Second, incorporating adversarial training not only obscures certain aspects of the original defense strategy's effectiveness but also introduces additional challenges. It is less effective against future advanced attacks, increases the difficulty of fine-tuning, and degrade inference performance [54]. Additionally, adversaries can adapt their attack models using similar adversarial strategies, reducing the overall effectiveness of the defense [25]. Thus, while these methods enhance defense performance, their implementation requires careful consideration of computational resources, model adaptability, and suitability for specific application scenarios. SiftFunnel belongs to NND & IB-based defense, and to explore and compare the original effectiveness of defense, our experiments excluded adversarial training while evaluating the trade-offs among usability, privacy, and deployability.

### 3 THREAT MODEL

#### 3.1 Knowledge background of adversary

**Attack scenarios.** Based on the adversary's level of knowledge, attack scenarios can be categorized into the following three types:

- (1) **White-box Scenario:** The adversary has complete white-box knowledge of the edge model, including its architecture, parameters, and gradient information.
- (2) **Black-box Scenario:** The adversary has only black-box access to the model, restricting their capability to observing the intermediate features. Additionally, their understanding of the edge model's architecture is restricted to prior knowledge or incomplete assumptions.
- (3) **Gray-box Scenario:** The adversary has partial knowledge of the edge model's architecture but remains unaware of defensive modifications, such as increased hidden layers.

The gray-box scenario enables the adversary to leverage their partial understanding of the edge model's architecture to enhance the capability of their attack model. For instance, if the defender partitions the first three convolutional layers of a ResNet-18 model [18] and further deepens the network, while the adversary is only aware of the original ResNet-18 architecture, they can only construct an approximate attack model based on partial knowledge of the initial three layers. However, in this scenario, adversaries can address this limitation by utilizing their understanding of the edge model's architecture and reasoning about its mapping capabilities to refine their attack model.

#### Knowledge shared by adversaries in different scenarios.

First, the adversary is assumed to understand the edge model's core task. To enhance their capability, the attack model in Gen-based MIA is trained on data distributions closely matching the target distribution, as detailed in Section 6.1. Second, the adversary has access to lossless transmission features and their dimensional distribution, which are essential for attack, as integrity of features and distribution facilitate the optimization of the MIA loss function and enhance the training of the attack model.

This study focuses on image classification tasks but emphasizes that the defense methods are applicable to other tasks where the edge model primarily handles feature extraction. Because tasks like segmentation, detection, and classification both rely on features processed by the edge model, MIA and defense strategies are not constrained by task-specific differences. Prior work [3] has also demonstrated input reconstruction and defense effectiveness in object detection using Gen-based MIA.

Moreover, image data, due to its high dimensionality, is especially vulnerable to MIAs, as shallow convolutional layers retain more redundant information [18, 56]. This makes defenses in image-based tasks more demonstrable. In contrast, textual data, with its strong contextual dependencies and syntactic complexity, has shown limited success in existing researches for achieving high-quality MIA reconstructions [7, 55]. This work focuses on image data to explore privacy-preserving techniques, leveraging its interpretability and the intuitive nature of defense effectiveness to validate the proposed methods.

#### 3.2 Attack strategy of the adversary

In the white-box attack scenario, the adversary can perform attacks using the MLE-based MIA method proposed in [19, 20]. To ensure the experiments are both comparative and representative, hyperparameter adjustments were made to achieve performance closer to optimal.

In the black-box attack scenario, the adversary can employ methods from [19, 51, 52], relying solely on output features for reverse mapping without access to the edge model's internal details. When protected by NND & IB-based defenses, the adversary lacks knowledge of architectural changes and must design the attack model based on prior assumptions.

In the gray-box attack scenario, the adversary can employ black-box strategies while leveraging known architectural information to optimize the attack model. This allows the reverse mapping capability to adapt to changes in the edge model. Detailed designs and training procedures for the attack models are provided in Section 6.

### 4 THEORETICAL ANALYSIS OF MIA IN CI

This section analyzes key factors affecting MIA effectiveness in collaborative inference, introduces a formulaic representation of its principles, and establishes a difficulty criterion from an information-theoretic perspective. We validate this criterion through experiments and use it to guide the design of SiftFunnel.

#### 4.1 Principles analysis of MIA

MIAs are categorized into MLE-based and Gen-based methods, both aiming to reconstruct input data using the output of edge model. MLE-based MIA calculates the loss between transmitted features and the output, then iteratively applies gradient descent to optimize the input, achieving reconstruction of the original data. The attack principle is formulated as follows:

$$\begin{aligned} x^{(k+1)} &= x^{(k)} - \eta \nabla_x \mathcal{L} \left( x, f_{\text{edge}} \left( x^{(k)} \right), z \right), \\ x^* &= \arg \min_x \mathcal{L} \left( x, f_{\text{edge}} \left( x^{(k)} \right), z \right) \end{aligned} \quad (3)$$

Where  $x^{(k)}$  represents the input value at the  $k$ -th iteration, typically initialized as gaussian noise, zeros, or ones.  $x^*$  denotes the final reconstructed result,  $z$  represents the transmitted features of the target input.  $f_{\text{edge}}(\cdot)$  refers to the target edge model,  $\nabla_x \mathcal{L}$  is the gradient calculated from the loss function and edge model parameters to optimize  $x$ , and  $\eta$  is the step size for each update.

According to [19], the loss function combines the  $l_2$  distance between  $f_{\text{edge}} \left( x^{(k)} \right)$  and  $z$  with a TV regularization term for  $x$ , forming the basis of rMLE-based MIA. The method relies on gradient descent, where the loss values depend on output features and gradients are computed using the target model's parameters.

To achieve effective attacks, sufficient output feature information  $\delta(z)$  and a well-chosen loss function are essential to ensure optimization space. Additionally, white-box knowledge of the edge model is required, as complex model mappings and limited feature information increase the risk of gradient descent converging to local minima [42, 56]. For instance, if two similar images produce nearly indistinguishable output features, reconstruction becomes challenging.

When dealing with complex edge model mappings or models protected by defense techniques, directly computing gradients in MLE-based MIA can significantly hinder optimization performance. To address this, He et al. [19, 20], building on the method from [51], developed a reverse mapping network for the edge model, which is categorized as Gen-based MIA. The key idea is to use a generator to approximate the reverse mapping of the edge model. Different methods adopt various strategies to train the generator. For instance, Yang et al. [51] trained a decoder using auxiliary task-related datasets, while Yin et al. [52] utilized intercepted feature data for training. The principle of this attack is summarized as follows.

$$G = \arg \min_G \mathbb{E}_{x' \sim p(x')} \mathcal{L} \left( G \left( f_{\text{edge}}(x') \right), x' \right), \quad (4)$$

$$x^* = G(z)$$

Where  $x'$  represents samples from an auxiliary data distribution  $p(x')$ . The loss function, typically mean square error, measures the distance between  $x'$  and the reconstructed data  $G(f_{\text{edge}}(x'))$  or  $z = f_{\text{edge}}(x')$ . The trained generator  $G$  must achieve the desired mapping  $G \approx f_{\text{edge}}^{-1}$  to reconstruct  $x^*$ .

The above formula highlights the conditions required for effective attacks:

- (1) A well-matched training dataset aligned with the target task, ideally with a distribution similar to the target dataset [51].
- (2) Sufficient and highly separable input information for the generator.

The rationale is that if the information in  $f_{\text{edge}}(x')$  is insufficient or cannot independently represent  $x'$ 's features, the loss in (4) will struggle to converge as  $G(f_{\text{edge}}(x'))$  remains ambiguous, limiting its training. These conditions must be met simultaneously. For instance, even with random feature drops, if the remaining features effectively distinguish inputs, the attack can still achieve satisfactory reconstruction [20]. Such frameworks resemble DAE [14], where the decoder can adapt to noise or feature drops.

Gen-based MIA demonstrates superior reconstruction performance compared to MLE-based MIA in defense scenarios. First, it avoids relying on model parameters for gradient computation, eliminating challenges from non-convex optimization. Second, it depends only on the output of the edge model, offering greater flexibility. Furthermore, existing defenses struggle to effectively remove redundant feature information, allowing Gen-based MIA to overcome defenses if the generator is capable of learning the edge model's reverse mapping.

## 4.2 Difficulty criterion for MIA in CI

We summarized the factors influencing MIA effectiveness using a formulaic representation. To further evaluate the difficulty of MIA implementation, we will formalize and analyze these factors from an information-theoretic perspective to establish a clear criterion.

First, the mutual information between the input  $x$  and the feature  $z$ ,  $I(x; z)$ , can be expressed as:

$$I(x; z) = H(x) - H(x | z) = H(z) - H(z | x) = H(z) \quad (5)$$

Where  $H(x | z)$  represents the conditional entropy of input  $x$  given  $z$ , and  $H(z | x)$  represents the reverse. Since there is no uncertainty in the mapping from  $x$  to  $z$  through  $f_{\text{edge}}$ ,  $H(z | x)$  is zero.

From Equation (5), we observe that complex mappings and information loss during neural network forward propagation reduce  $I(x; z)$  and increase  $H(x|z)$ , making non-convex optimization with backpropagation more difficult. Consequently, this increases the challenge for MLE-based MIA to reconstruct  $x$  from  $z$ .

An inappropriate loss function or insufficient output information can increase  $H(x|z)$  while reducing  $H(z)$  and  $\delta(z)$ . Notably, a low  $\delta(z)$  does not necessarily correspond to a low  $H(z)$ . For example, even if 80% of  $z$ 's elements are randomly dropped,  $H(z)$  may still remain high [20]. Thus, the performance of MLE-based MIA is directly affected by  $H(x|z)$ ,  $H(z)$ , and  $\delta(z)$ .

To further illustrate the influence of mutual information and entropy on the difficulty of MIA, we can derive the following relationship for any  $x \rightarrow z \rightarrow x^*$  using Fano's inequality [2, 49]:

$$H(P_e) + P_e \log |\mathbb{X}| \geq H(x | x^*) \geq H(x | z) \quad (6)$$

where  $P_e = \text{Prob}\{x \neq x^*\}$ ,  $x^*$  is the reconstruction by MIA, and  $\mathbb{X}$  denotes the value space of  $x$ .

Since  $\mathbb{X} \geq 2$  and  $H(P_e) \leq 1$ . Therefore inequality (6) can be written as

$$P_e \geq \frac{H(x | z) - 1}{\log |\mathbb{X}|} = \frac{H(x) - I(x, z) - 1}{\log |\mathbb{X}|} = \frac{H(x) - H(z) - 1}{\log |\mathbb{X}|} \quad (7)$$

Since  $H(x)$  and  $|\mathbb{X}|$  are influenced by training data, they are typically assumed to be objective and invariant. Therefore, we observe that increasing the lower bound of  $P_e$ , and thus the difficulty of MIA, is influenced by  $H(x|z)$ ,  $H(z)$ , and  $I(x, z)$ .

From Equation (4), Gen-based MIA requires sufficient input information  $\delta(z)$  and high  $H(z)$  to ensure maximum separability and enable loss convergence, allowing the generator to simulate reverse mapping effectively. A larger  $\delta(z)$  not only facilitates generator training but also directly impacts the reconstruction of  $x^*$ . The relationship in Inequality (7) is also applicable here.

The validity of related research can also be explained by both. For example, [51] reduces  $\delta(z)$  by pruning output information, disrupting training and reconstruction, while [57] increases entropy via non-linear functions to enhance generator performance. Thus,  $H(z)$  and  $\delta(z)$  are critical factors influencing Gen-based MIA.

The analysis indicates that the difficulty of implementing both types of MIA is inversely proportional to the mutual information, entropy, and output information. Therefore, the difficulty criterion for MIA can be formulated as follows, where  $k_1$  and  $k_2$  are proportionality constants:

$$D_{\text{mia}} \propto \left( \frac{k_1}{\{I(x; z); H(x | z); H(z)\}} + \frac{k_2}{\delta(z)} \right) \quad (8)$$

Based on this criterion, existing defenses [10, 34, 45] using the information bottleneck theory can be understood as approximating a reduction in  $I(x; z)$  through various algorithms to increase the difficulty of MIA. Perturbation-based defenses [20] aim to directly increase  $H(x|z)$ . The defensive effect of deeper neural networks [3, 8] can be explained by their ability to reduce  $I(x; z)$  and  $\delta(z)$ . This is mainly because, without skip connections [17], mutual information progressively decreases during forward propagation in neural networks. In contrast, residual networks with skip connections add

the output of one layer to its input, which may prevent  $\delta(z)$  from decreasing and, in some cases, even cause it to increase.

### 4.3 Demonstration and Guidance for Defense

To validate  $D_{mia}$  and the theoretical analysis, we designed experiments using a CNN that progressively reduces the spatial size while increasing the channel size, based on the framework in [18, 51], and ResNet-18 with skip connections, quantifying each block. We trained MINE [4] on the same dataset used to train the full model  $f$  to estimate the lower bound of  $I(x, z)$ . The core idea of MINE is to optimize a neural network estimator using the Donsker-Varadhan (DV) representation [9] as the loss function, providing an approximate estimate of the mutual information between random variables.

Mutual information is defined as follows:

$$I(X; Z) = \mathbb{E}_{p(x,z)} \left[ \log \frac{p(x,z)}{p(x)p(z)} \right] \quad (9)$$

Where  $p(x, z)$  represents the joint distribution, existing defense methods approximate it, but limited batch sizes lead to inaccuracies and variations in estimates. For high-dimensional data (e.g., images), accurate estimation requires many samples.

To avoid direct distribution estimation, the DV representation reformulates mutual information as an optimization problem:

$$I(X; Z) \geq \sup_T \mathbb{E}_{p(x,z)} [T(x, z)] - \log \mathbb{E}_{p(x)p(z)} \left[ e^{T(x,z)} \right] \quad (10)$$

Where  $T$  is a learnable function, this formulation enables  $I(X; Z)$  to be estimated by optimizing  $T$  to obtain a lower bound.

MINE achieves this by parameterizing  $T$  with a neural network  $T_\theta$  and maximizing the DV bound through gradient descent to approximate mutual information:

$$\hat{I}(X; Z) = \mathbb{E}_{p(x,z)} [T_\theta(x, z)] - \log \mathbb{E}_{p(x)p(z)} \left[ e^{T_\theta(x,z)} \right] \quad (11)$$

As shown in Figure 2, we trained the target models on the CIFAR-10 [26] and used Equation (11) to train MINE for the corresponding blocks. Figures 2(a, b) show that increasing network depth reduces both mutual information and effective information, leading to a decrease in attack performance. Figures 2(c, d) illustrate that while skip connections within two layers do not reduce  $\delta(z)$ , they slightly lower  $I(x, z)$ , moderately affecting attack performance.

Previous research [17] identified vulnerabilities caused by skip connections in centralized MIA. Our study further highlights their impact on MIA effectiveness in CI. Transmission between layers in ResNet alters feature channels and dimensions, requiring a shortcut layer, leading to a more pronounced decline in mutual information compared to direct stacking within layers. This, in turn, degrades MIA performance and aligns with our criterion.

Notably, while mutual information at ResNet’s fourth layer is higher than that at CNN’s second layer, MLE-based MIA does not perform better. This stems from the fact that these methods rely heavily on gradient descent, making them sensitive to suboptimal optimizers, hyper-parameter settings, and deeper network structures, which hinder gradient calculations for optimizing  $x$ . The lack of flexible and efficient methods for MLE-based MIA remains a gap in current research, often leading to their exclusion in defense evaluations—a topic warranting further exploration [8]. In our experiment and Section 6, we still evaluate MLE-based MIA

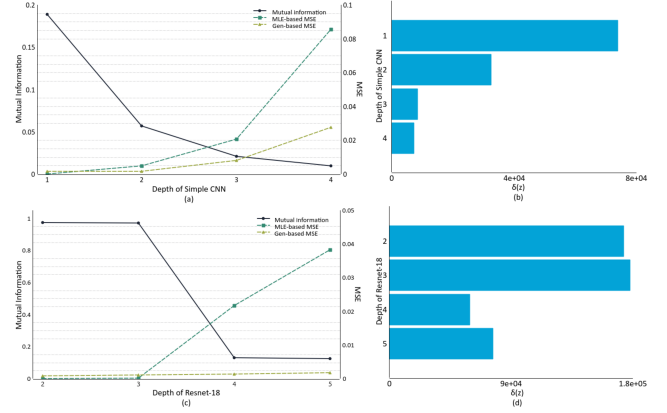


**Figure 2: The impact of neural network depth on  $I(x, z)$ ,  $\delta(z)$ , as well as MLE & Gen-based MIA.**

against various defenses and provide evidence demonstrating the effectiveness of our method in defending against such attacks.

In conclusion, through theoretical analysis and experimental validation, we established  $D_{mia}$  and determined that effective defense strategies must impact mutual information, entropy, and  $\delta(z)$ . The following considerations can guide defense design:

- Since  $I(x, z)$  is challenging to compute and current algorithms lack flexibility and efficiency, defenses should focus on indirectly influencing  $H(x | z)$  and  $H(z)$ .
- The design of edge models should strategically affect  $H(z)$  and  $\delta(z)$ .
- For practical applications, the light-weighting of edge models should balance usability with their impact on the factors outlined in the criterion.

## 5 SIFTFUNNEL: INFORMATION SIFTING FUNNEL

Building on the theoretical analysis, criterion, and experiments in Section 4, this section introduces SiftFunnel and its adherence to  $D_{mia}$  in edge model and loss function design. We first outline the core principles and objectives of SiftFunnel. Then, we detail the edge model’s structure, key modules, and role in the forward propagation of information. Finally, we explain the loss function’s impact on  $H(x | z)$ ,  $H(z)$  and  $\delta(z)$ , highlighting its ability to extract useful information while minimizing redundancy and increasing the uncertainty of  $z$  to  $x$ .

### 5.1 Overview of SiftFunnel

Guided by  $D_{mia}$ , SiftFunnel aims to balance usability and privacy in edge models by increasing the uncertainty of inferring  $x$  from  $z$  while reducing  $z$ ’s information and separability. To this end, as shown in Figure 3, we introduce two key improvements: First, the edge model is enhanced by modifying the final hidden layer into a funnel-shaped structure and incorporating attention modules between layers. Second, the loss function is optimized to ensure that model training balances usability with privacy protection.

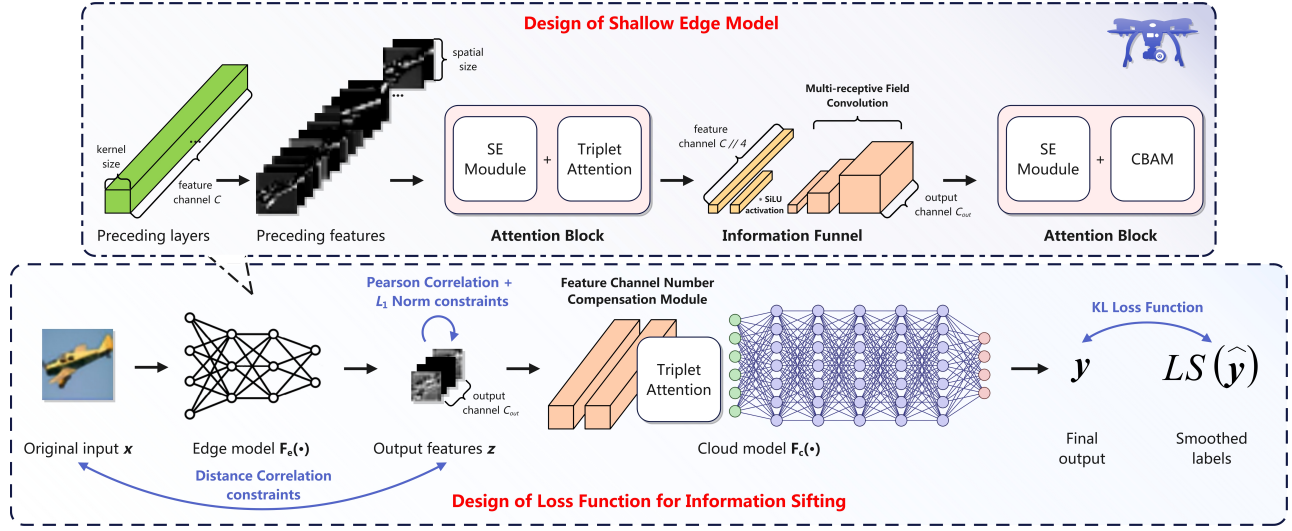


**Figure 3: Overview of SiftFunnel. Specifically, the design is divided into two aspects: the architecture and the loss function for the edge and cloud model.**

Specifically, in the edge model design, the final layer adopts a funnel-shaped structure, reducing feature channels while preserving spatial dimensions. This reduces computation, lightens the edge device load, and limits redundant information. Attention mechanisms and multi-receptive field convolutions enhance task-relevant information, while a feature channel supplementation module in the cloud model ensures task accuracy. With the improved edge model, designing an effective loss function is essential. To reduce redundancy,  $I(x, z)$  and increasing the uncertainty of  $z$  to  $x$ , we use Distance Correlation [27] for nonlinear correlations and the Pearson Coefficient [6] with  $l_1$ -norm for linear correlations. Additionally, Label Smoothing (LS) and Kullback-Leibler (KL) divergence [9] ensure model accuracy, enhancing usability while reducing the separability of  $z$ .

## 5.2 The Design of Shallow Edge Model

**Information Funnel.** Deepening the neural network enhances feature extraction and reduces  $I(x, z)$ , as confirmed in Section 4. Previous work [21] shows through Fisher information [36] that deeper networks improve task relevance and resist MIA. Inspired by this, we redesign the final layer of the edge model with an Information Funnel module. This module reduces output channels to one-fourth in the first layer and further in the second layer, with channel selection based on the spatial size of feature maps. If the spatial size is reduced significantly, channels can exceed 10 to maintain accuracy. If unchanged, channels can be set to 2 to limit redundancy while preserving accuracy. Adjusting channels based on spatial size is necessary because spatial information loss is irreversible, whereas channel information loss can be compensated in the cloud model. This compensation increases  $I(z, y)$  without reversing the reduction in  $I(x, z)$ , maintaining high attack difficulty as shown in Section 6.3. So, we add the channel compensation module in the cloud model to guarantee usability. Importantly, assumption about extracting features from non-independent transmission modules are idealized,

requiring adversaries to have full white-box knowledge of the cloud model as if they were the developer.

The Information Funnel’s channel structure controls output but does not limit redundancy or enhance task-relevant information transmission, affecting usability. Inspired by Inception networks [44], we redesign it as a multi-receptive field convolutional framework with three low-channel layers. A  $1 * 1$  kernel fuses channel information, followed by  $3 * 3$  and  $5 * 5$  kernels to expand the receptive field, extract richer task-relevant features, improve decision-making, and reduce mutual information with  $x$ , while lowering parameters of the edge model and controlling  $\delta(z)$ .

**Attention Block.** To enhance the output of task-relevant information from the Information Funnel, attention modules are incorporated both before and after it. The first block combines an SE block [23] and Triplet Attention [32]. The SE block evaluates the contribution of information within each channel, suppressing channels with low task relevance. Triplet Attention reduces spatial information while maintaining smooth, continuous outputs, preserving fine-grained features for further processing. The second block integrates SE and CBAM modules [48]. Compared to Triplet Attention, CBAM is a lightweight module that sequentially calculates channel and spatial weights to enhance or suppress input features. Since CBAM’s channel and spatial attention are independently designed, certain weights are suppressed redundantly, resulting in sparser outputs. This sparsity is beneficial for output processing, effectively increasing  $H(x | z)$  while reducing  $H(z)$  and  $\delta(z)$ .

## 5.3 The Design of Loss Function

To further enhance model usability and data privacy, a appropriately designed loss function is essential to guide the training process.

To reasonably increase  $H(x | z)$  and suppress  $H(z)$  within the edge model structure, loss constraints must be applied to  $x$  and  $z$ . The key challenge is that, without intervention, neural networks



may retain irrelevant input information in their output during forward propagation. This information, which does not significantly impact decision-making, reduces the difficulty of MIAs by maintaining the mutual information and entropy.

Some defense approaches utilize Constrained Covariance (COCO) [16] to estimate correlation, focusing primarily on the linear relationship between  $x$  and  $z$ . However, since neural networks predominantly perform nonlinear operations, studies have shown that this constraint is not only ineffective but may also lead to reduced usability [34]. Alternatively, some approaches employ the Hilbert-Schmidt Dependency Criterion (HSIC) [15] to estimate correlation. However, kernel-based calculations in HSIC rely heavily on the appropriate selection of  $\sigma$ . Improper  $\sigma$  value can introduce bias in nonlinear correlation estimation, limiting the generalizability of this method and reducing its effectiveness across various scenarios.

**Nonlinear correlation constraint.** We observe that shallow neural network features retain significant similarity to the input and are derived through nonlinear operations. To address this, we use distance correlation to measure the non-linear relationship between  $x$  and  $z$ , incorporating it as a loss constraint. This helps remove redundant input information from the output, and effectively increase  $H(x | z)$ . The calculation of distance correlation is as follows:

$$\mathcal{L}_{d\text{Cor}} = d\text{Cor}(x, z) = \frac{d\text{Cov}(x, z)}{\sqrt{d\text{Var}(x) \cdot d\text{Var}(z)}} \quad (12)$$

Where  $d\text{Cov}(x, z)$  represents the distance covariance between  $x$  and  $z$ , and the denominator is the product of the distance variances for the two samples.

To compute the numerator, a distance matrix  $A$  is first calculated, where each element is the Euclidean distance between samples, defined as  $A = \|x_i - x_j\|_2$ . To remove the influence of sample shifts, the distance matrix is centered as  $A_{ij}^c = A_{ij} - \bar{A}_i - \bar{A}_j + \bar{A}$ , where  $\bar{A}_i$  denotes the mean of the  $i$ -th column, and similar operations apply to other terms. With the centered distance matrix, the distance covariance is computed as  $d\text{Cov}(x, z) = \frac{1}{n^2} \sum_{i,j} A_{ij}^c B_{ij}^c$ , where  $B$  represents the matrix of features  $z$ , and  $n$  denotes the batch size.

The distance variances is defined as  $d\text{Var}(x) = \frac{1}{n^2} \sum_{i,j} A_{ij}^c{}^2$ , which normalizes the distance covariance. The value range of distance correlation is  $[0, 1]$ , where 1 indicates perfect correlation. Since  $x$  and  $z$  exhibit high distance similarity and are derived through nonlinear operations, distance correlation is well suited as a constraint term. Moreover, as a distribution-free measure, it does not rely on specific data distributions, making it effective for non-Gaussian distributions, nonlinear relationships, and complex data types such as images and text. For non-stationary and multimodal data, distance correlation provides stable dependency measurements, allowing the constraint to flexibly adapt to different models and data.

**Linear correlation constraint.** In addition to constraining the loss between  $x$  and  $z$ , it is necessary to design loss constraints specifically for the  $z$ . The primary issue lies in the  $z$  containing repetitive or similar information, which is redundant for decision-making and provide additional input for Gen-based MIAs, strengthening local constraints in the input space and improving reconstruction accuracy.

To address this, we propose using the Pearson correlation coefficient as a loss constraint to reduce the linear correlation within features  $z$ , effectively eliminating redundant information and entropy. The calculation is as follows:

$$\mathcal{L}_{\text{Pearson}} = \frac{1}{C^2} \sum_{c_1=1}^C \sum_{c_2=1}^C (\text{pCor}_{c_1, c_2})^2 = \frac{1}{C^2} \sum_{c_1=1}^C \sum_{c_2=1}^C \left( \frac{\text{Cov}_{c_1, c_2}}{\sigma_{c_1} \cdot \sigma_{c_2}} \right)^2 \quad (13)$$

Where  $\text{Cov}_{c_1, c_2}$  represents the covariance matrix between channels  $c_1$  and  $c_2$ , calculated as  $\text{Cov}_{c_1, c_2} = \frac{1}{H \cdot W} \sum_{i=1}^{H \cdot W} (z_{c_1, i} - \mu_{c_1}) \cdot (z_{c_2, i} - \mu_{c_2})$ , where  $z_{c_1, i}$  is the  $i$ -th element of channel  $c_1$  and  $\mu_{c_1}$  is its mean.  $H$  and  $W$  denote the height and width of the feature space.  $\sigma_{c_1}$  and  $\sigma_{c_2}$  are the standard deviations, calculated as

$$\sigma_{c_1} = \sqrt{\frac{1}{H \cdot W} \sum_{i=1}^{H \cdot W} (z_{c_1, i} - \mu_{c_1})^2}$$

To compute the scalar  $\mathcal{L}_{\text{Pearson}}$ , the squared correlations of all channel pairs are averaged, keeping the value range within  $[0, 1]$ . This avoids negative values, which could lead to suboptimal updates during gradient descent. With negative values might drive correlations toward complete negative correlation, introducing unnecessary redundancy or unsuitable learning patterns, and hindering convergence. Therefore, the goal is to minimize the coefficient toward zero, as lower values indicate reduced linear correlation. Using the squared correlations and their average ensures a smoother and more stable gradient descent process.

Additionally, to prevent extreme values in the feature output weights during the optimization of the above constraints, we include the  $l_1$ -norm as a loss term. This term is added specifically to suppress weights, but excessive emphasis on it could interfere with normal model training. Therefore, the coefficient  $\tau$  for this loss term is set below  $1e-2$  to balance its influence.

**Label smoothing.** Finally, to ensure model usability, we draw inspiration from [43] and apply LS to refine the target loss, as shown in the formula (14). Additionally, KL divergence is used instead of cross-entropy (CE) as the primary loss function for optimization.

$$LS(\hat{y}_c) = 1 - \alpha + \frac{\alpha}{K}, \quad LS(\hat{y}_i) = \frac{\alpha}{K} \quad (14)$$

Where  $LS(\hat{y}_c)$  refers to the label smoothing element under the target class,  $LS(\hat{y}_i)$  is the  $i$ -th element of the non-target class.  $\alpha$  is smooth factor and  $K$  is the total number of categories.

CE emphasizes enhancing inter-class feature distinctions, while KL divergence as a loss function supports smoother and more generalized feature extraction between classes [43]. Within-class feature extraction focuses on capturing universal characteristics, ensuring the model maintains a certain level of generalization and robustness for the target task. Moreover, this optimization reduces maximum feature separability, increasing the difficulty of attack, as demonstrated in Section 6.

In summary, the proposed loss function first applies nonlinear correlation constraints between input  $x$  and features  $z$  to increase  $H(x | z)$  and suppress  $H(z)$ . Second, it imposes linear correlation and extreme value constraints on  $z$  to further enhance  $H(x | z)$  and suppress  $\delta(z)$ . Finally, LS and KL divergence is applied to the target loss to maintain usability while slightly suppressing  $H(z)$ . The final formulation of this optimization is as follows, with specific

parameter settings referenced in Section 6.

$$\min \mathcal{L}_\theta(x, z, \hat{y}) = \lambda_1 \cdot KL(f(x), LS(\hat{y})) + \lambda_2 \cdot \mathcal{L}_{dCor} + \lambda_3 \cdot \mathcal{L}_{Pearson} + \tau \cdot \|z\|_1 \quad (15)$$

## 6 EXPERIMENTS

In this section, we systematically evaluate and compare the ability of SiftFunnel and existing approaches to resist MIA. The results are analyzed from three perspectives: the impact of defense methods on  $I(x, z)$  and  $\delta(z)$ , the influence of datasets and model architectures, and ablation studies. The specific experimental setup and evaluation metrics are shown below.

### 6.1 Experimental Setup

1) *Datasets*. We used three types of image recognition datasets, with processing details outlined as follows. The detailed data allocation is shown in Table 1.

- **CIFAR-10** [26]. The CIFAR-10 dataset consists of 60,000 RGB images categorized into ten classes with an original resolution of  $32 \times 32$ . To make the results clearer and more intuitive, we used an unscaled resolution of  $64 \times 64$ .
- **FaceScrub** [33]. FaceScrub is a URL dataset with 100,000 images of 530 actors, which contains 265 male actors and 265 female actors. However, since not every URL was available during the writing period, we downloaded a total of 43,149 images for 530 individuals and resized the images to  $64 \times 64$ .
- **CelebA** [29]. CelebA is a dataset with 202,599 images of 10,177 celebrities. We used the same crop as [51] to remove the background of images in this dataset other than faces to reduce the impact on the experiment. In order to eliminate individual overlap, we removed a total of 6,878 images of 296 individuals and similarly resized the images to  $64 \times 64$ .
- **ChestX-ray** [38]. This dataset is a curated collection of COVID-19 chest X-ray images compiled from 15 publicly available datasets. It contains 1,281 COVID-19 X-rays, 3,270 normal X-rays, 1,656 viral pneumonia X-rays, and 3,001 bacterial pneumonia X-rays. For our analysis, we converted the images to gray scale with a resolution of  $128 \times 128$ .

2) *Attack Method*. The selection of attack methods has been discussed in Section 3.2. Specifically, for MLE-based MIA, this paper has adjusted to the hyper-parameter values that yield the best results. For Gen-based MIA, the attack model in this paper is designed as the inverse architecture of the edge model. Moreover, under the gray-box scenario assumption, the attack model can enhance the expressive power of the reverse mapping as the edge model architecture changes. The attack model is trained using the Adam optimizer with a learning rate of  $2e-4$ , a  $\beta_1$  of 0.5, and a ReduceLROnPlateau scheduler with a factor of 0.5 and patience of 20. The

**Table 1: Data allocation of the target model and attack model.**

Classifier		Attack Model
Task	Data	Auxiliary Data
CIFAR-10 (10 classes)	Train: 66.6%, Test: 16.7%	16.7% (10 classes of CIFAR-10)
FaceScrub (530 classes)	Train: 80%, Test: 20%	CelebA (non-individual overlapping)
ChestX-ray (4 classes)	Train: 66.6%, Test: 16.7%	16.7% (4 classes of ChestX-ray)

attack model training is based on strong assumptions, as shown in Table 1, and only the models with the minimum test MSE are saved to highlight the defense’s effectiveness.

3) *Target Edge Model and Implementation Details*. We employ the same comprehensive model architecture as detailed in [51], comprising four CNN blocks succeeded by two fully connected layers. This model is trained using the Adam optimizer with a learning rate of  $2e-4$ , a  $\beta_1$  parameter of 0.5, and a ReduceLROnPlateau scheduler with a reduction factor of 0.5 and patience of 25. Each CNN block is composed of a convolutional layer, a batch normalization layer, a max-pooling layer, and a ReLU activation function. The target edge model encompasses the initial two CNN blocks. For the training of the edge model protected by SiftFunnel, we have specified the parameters  $\lambda_1$  to 3.5,  $\alpha$  to 0.35,  $\lambda_2$  to 0.8, and  $\lambda_3$  to 0.6 in Equation (15). In addition to this, to argue the impact of the model architecture for the defense, we use different CNNs as follows: (1) VGG16 adapted from [41]; (2) ResNet-18 adapted from [18], the learning rates are  $3e-4$ . The division positions of resnet and vgg are not fixed. For detailed accuracy and how to divide them, see Section 6.3 for analysis. All experiments were performed on two RTX 4090 GPUs and an Intel Core i9-14900KF  $\times 32$  CPU.

4) *Comparison of Defense Methods*. We will compare three existing categories of defense methods. For Perturbation-based defenses, we select **Adding noise & Dropping features** [20], **DPSGD** [1], and negative label smoothing (**NLS**) [43]. For IB-based defenses, we choose **MID** [45], **BiDO** (with HSIC) [34], **VIB** [47], and **InfoSCISORS** [10]. For NND & IB-based defenses, we opt for **AE-based protection** [3]. Our method falls into the NND & IB-based defense category, which also requires analyzing the defensive effect in a gray-box scenario. Furthermore, all comparison methods have been selected and set with appropriate hyper-parameters for comparison, with detailed settings found in Section 6.3 analysis. Lastly, all methods are trained without adversarial training, focusing solely on the effects of the original defense methods.

### 6.2 Evaluation Metrics

We have selected 7 evaluation metrics to assess usability, privacy, and deployability. For usability assessment, we employ **Test Accuracy (Test ACC)**, which evaluates the final performance of the model protected by defense techniques on the test dataset. Regarding privacy assessment, we initially utilize **MSE**, **Peak Signal-to-Noise Ratio (PSNR)**, and **Structural Similarity Index (SSIM)** to evaluate the effectiveness of MIA on reconstructing the input data of the protected model [52]. Here, a higher MSE and lower PSNR and SSIM (ranging from 0 to 1) indicate better defense effectiveness. In addition to these, we also employ MINE [4], as mentioned in Section 4.3, to assess **Mutual Information (MI)** (ranging from 0 to 1) and the **Effective Information Mean**  $\delta(z)$ , which is the mean of the non-zero output by the edge model on the test dataset. The specific training methods and model architecture for MINE are referenced from xxx. For deployability, we consider the **Edge model’s parameter count**  $|\theta_{\text{edge}}|$  and Inference Latency. The model parameter count directly determines memory or GPU memory occupation, while inference latency is tested on both CPU and GPU.

**Table 2: Quantitative evaluation of CNN on CIFAR-10 with different defenses against two MIAs.  $\uparrow$  indicates higher is better,  $\downarrow$  indicates lower is better. Bolded values are the best. Blue highlights show unprotected baseline performance, red indicates increased edge device load, yellow indicates reduced load, and gray shows gray-box defense performance.**

Method Class	Method	Test ACC $\uparrow$	MLE-based Attack [18]			Gen-based Attack [20]			MI $\downarrow$	$\delta(z)\downarrow$	$ \theta_{\text{edge}} \downarrow$
			MSE $\uparrow$	PSNR $\downarrow$	SSIM $\downarrow$	MSE $\uparrow$	PSNR $\downarrow$	SSIM $\downarrow$			
Unprotected		88.28%	0.0045	28.3421	0.9883	0.0017	32.5498	0.9987	0.0566	32,549	299,520
Perturbation-based	Adding noise [20] ( $\sigma = 0.8$ )	74.85% (-13.43%)	0.0291	20.1511	0.9135	0.0172	22.4249	0.9299	0.0502	65,535	299,520
	Dropping [20] ( $r = 0.8$ )	21.18% (-67.10%)	0.0127	23.7340	0.9609	0.0135	23.4835	0.9481	0.0501	6,509	
	DPSGD [1] (20, $1e-5$ )	61.83% (-26.45%)	0.0218	21.3868	0.9479	0.0016	32.4800	0.994	0.0623	39,829	
	NLS [43] ( $\alpha = -0.05$ )	87.60% (-0.68%)	0.0002	42.2684	0.9996	0.0014	33.3732	0.9949	0.0573	47,183	
IB-based	MID [45] ( $1e-2$ )	81.53% (-6.75%)	1.74e-5	50.4675	0.9999	0.0013	34.5184	0.9967	0.0584	45,198	299,520
	BiDO [34] (2; 20)	84.12% (-4.16%)	0.6699	6.5111	0.0138	0.035	19.2965	0.8751	0.0429	3,345	
	VIB [47]	88.21% (-0.07%)	0.5552	7.3264	0.0358	0.0042	28.5054	0.9842	0.0551	18,069	
	InfoSCISSORS [10]	83.46% (-4.83%)	0.5715	7.2007	0.1345	0.0062	26.8799	0.9948	0.0549	43,364	
NND & IB-based	AE-based [3]	<b>90.56% (+2.28%)</b>	0.6345	6.7472	0.0051	0.0542	17.4852	0.8151	0.0358	2,617	2,365,056
	<b>SiftFunnel</b>	85.49% (-2.79%)	<b>0.6792</b>	<b>6.4510</b>	<b>0.0051</b>	<b>0.1166</b>	<b>14.1112</b>	<b>0.5419</b>	<b>0.0167</b>	<b>1,006</b>	<b>14,911</b>

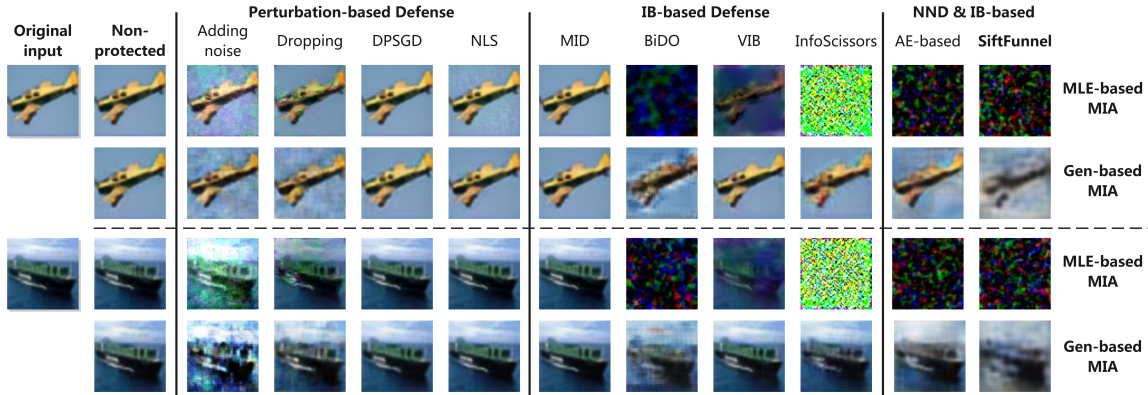


**Figure 4: A visual evaluation of the attack effectiveness of two MIAs on CNN edge models protected by various defense techniques, with NND & IB-based results specifically reflecting the gray-box scenario.**

### 6.3 Experimental Results

1) *The effect of various defenses on the MI and  $\delta(z)$ .* the effectiveness of defenses is reflected by MI and  $\delta(z)$ , aligning with the criterion  $D_{\text{mia}}$  and the theoretical analysis presented in Section 4. Specifically, unprotected edge models show significant vulnerability to input reconstruction under both types of MIAs, with MI at 0.0566, MSE below 0.01, and SSIM exceeding 0.98. When protected by Perturbation-based defenses, all methods except NLS exhibit over a 10% drop in Test ACC. Moreover, these methods achieve only an 11% reduction in MI at most, demonstrating clear weaknesses against both MIAs. NLS shows a slight increase in mutual information for shallow neural networks, leading to weaker resistance to both types of attacks. Under IB-based defenses, usability sees a slight decline, but all methods except MID provide strong resistance against MLE-based MIA, with MSE values exceeding 0.5. Among these techniques, only BiDO significantly impacts MI and  $\delta(z)$ , providing effective defense, but its parameter selection and kernel

width configuration (as shown in the table) are challenging, limiting its generalizability—a limitation further evidenced in subsequent experiments. This experiment adheres to the InfoSCISSORS setup, providing CLUB with a complete dataset and sufficient training iterations to ensure convergence. While CLUB effectively defends against MLE-based MIA, it struggles under the experimental conditions to resist Gen-based MIA and results in a 4.83% accuracy loss. Under AE-based defenses, target model usability improves, likely because the original model lacked sufficient capacity for optimal task classification, and the added model complexity enhanced performance. Additionally, MI indicates notable reductions in mutual information, showcasing reasonable defense effectiveness. However, in gray-box scenarios, AE-based defenses show reduced resistance, and the added complexity imposes a eightfold storage burden on edge models, as revealed by  $|\theta_{\text{edge}}|$ . SiftFunnel achieves the best defense performance against both MIAs while maintaining an accuracy loss below 3%. For MLE-based MIA, it achieves an MSE of 0.6792, and for Gen-based MIA, an MSE above

**Table 3: Quantitative evaluation of ResNet-18 on CIFAR-10 with different defenses against two MIAs. The target edge model is the first residual block of ResNet-18.  $\uparrow$  indicates higher is better,  $\downarrow$  indicates lower is better. Bolded values are the best. The meanings of color-coded regions are consistent with those in Table 2.**

Method Class	Method	Test ACC $\uparrow$	MLE-based Attack [18]			Gen-based Attack [20]			MI $\downarrow$	$\delta(z)\downarrow$	$ \theta_{\text{edge}} \downarrow$
			MSE $\uparrow$	PSNR $\downarrow$	SSIM $\downarrow$	MSE $\uparrow$	PSNR $\downarrow$	SSIM $\downarrow$			
Unprotected		90.43%	0.0001	71.0996	0.9991	0.0010	34.6599	0.9991	0.9719	182,134	149,824
Perturbation-based	Adding noise [20] ( $\sigma = 2$ )	81.39% (-9.04%)	0.0035	29.3354	0.9872	0.0054	27.4167	0.9794	0.9619	262,144	149,824
	Dropping [20] ( $r = 0.8$ )	14.09% (-76.34%)	0.0069	26.3641	0.9754	0.0077	25.9334	0.9711	0.9514	35,574	
	DPSGD [1] (20, $1e-5$ )	61.85% (-28.58%)	0.1901	11.9821	0.7172	0.0060	26.9751	0.9802	0.9515	178,956	
	NLS [43] ( $\alpha = -0.05$ )	88.57% (-1.86%)	0.0034	29.5001	0.9894	0.0011	34.4231	0.9961	0.9718	176,456	
IB-based	MID [45] ( $1e-2$ )	79.48% (-10.95%)	1.42e-7	73.2595	0.9999	0.0010	34.5893	0.9965	0.9729	173,587	149,824
	BiDO [34] (5; 10)	<b>90.08%</b> (-0.35%)	4.38e-7	68.3603	0.9999	0.0020	31.7621	0.9927	0.9647	219,832	
	VIB [47]	89.18% (-1.25%)	0.5869	7.0853	0.0216	0.0020	31.7621	0.9928	0.9402	54,800	
	InfoSCISSORS [10]	88.03% (-2.40%)	3.10e-5	49.8548	0.9999	0.0058	27.1608	0.9799	0.8927	216,919	
NND & IB-based	AE-based [3]	89.19% (-1.24%)	0.6543	6.6189	0.1243	0.0143	23.2332	0.9488	0.9397	74,356	279,136
	<b>SiftFunnel</b>	88.43% (-2.00%)	<b>0.6538</b>	<b>6.6166</b>	<b>0.0059</b>	<b>0.1957</b>	<b>11.8562</b>	<b>0.0793</b>	<b>0.4772</b>	<b>4,028</b>	<b>78,864</b>

**Table 4: Quantitative evaluation of different defense methods in protecting CNN against MIAs on the FaceScrub dataset. Changes in data types alter the inference task, requiring adjustments to the parameters of the defense methods.**

Method Class	Method	Test ACC $\uparrow$	MLE-based Attack [19]			Gen-based Attack [20]			MI $\downarrow$	$\delta(z)\downarrow$	$ \theta_{\text{edge}} \downarrow$
			MSE $\uparrow$	PSNR $\downarrow$	SSIM $\downarrow$	MSE $\uparrow$	PSNR $\downarrow$	SSIM $\downarrow$			
Unprotected		88.31%	0.0005	37.6115	0.9972	0.0006	32.4108	0.9908	0.0514	45,271	299,520
Perturbation-based	NLS [43] ( $\alpha = -0.2$ )	87.97% (-0.34%)	0.0004	38.8904	0.9980	0.0018	32.3274	0.9906	0.0496	44,783	299,520
IB-based	MID [45] ( $1e-2$ )	79.45% (-10.98%)	0.0017	32.3435	0.9897	0.0018	32.1285	0.9901	0.0507	39,277	299,520
	BiDO [34] (2; 20)	88.02% (-0.29%)	0.0004	39.0838	0.9978	0.0018	32.2048	0.9904	0.0493	44,915	
	VIB [47]	<b>88.05%</b> (-0.26%)	0.7354	6.1060	0.0032	0.0033	29.5697	0.9823	0.0493	15,649	
	InfoSCISSORS [10]	81.61% (-6.70%)	<b>0.7449</b>	<b>6.0504</b>	<b>0.0026</b>	0.0060	26.9803	0.9675	0.0408	57,050	
NND & IB-based	AE-based [3]	83.45 (-4.86%)	0.6474	6.6594	0.0090	<b>0.0609</b>	<b>16.9260</b>	<b>0.6656</b>	0.0238	<b>585</b>	2,365,056
	<b>SiftFunnel</b> ( $\lambda_1 = 5.0, \lambda_2 = 0.1, \lambda_3 = 0.1$ )	85.39% (-2.92%)	0.7264	6.1593	0.0060	0.0559	17.3018	0.6854	<b>0.0104</b>	637	<b>14,911</b>

**Table 5: Quantitative evaluation of the resistance to MIA across different architectures on CIFAR-10. The edge model divisions for CNN and ResNet-18 follow the configurations in Tables 2 and 3, while for VGG16, the edge model is set at the first ReLU layer after a max-pooling operation.**

Architecture	Test ACC $\uparrow$	MLE-based Attack [19]			Gen-based Attack [20]			MI $\downarrow$	$\delta(z)\downarrow$	$ \theta_{\text{edge}} \downarrow$
		MSE $\uparrow$	PSNR $\downarrow$	SSIM $\downarrow$	MSE $\uparrow$	PSNR $\downarrow$	SSIM $\downarrow$			
CNN	85.49% (-2.79%)	0.6792	6.4510	0.0051	0.1166	14.1112	0.5419	0.0167	1,006	14,911
ResNet-18	88.43% (-2.00%)	0.6538	6.6166	0.0059	0.0639	16.7314	0.7647	0.4772	4,028	78,864
VGG16	88.89% (-2.18%)	0.7801	5.8450	0.0005	0.1957	11.8562	0.0793	0.0128	3,587	52,086

0.1. In gray-box scenarios, it maintains an MSE of 0.06 and an SSIM of 0.7647, ensuring robust resistance. Furthermore, MI and  $\delta(z)$  demonstrate that SiftFunnel exerts optimal influence on the key elements of  $D_{\text{mia}}$ . Additionally,  $|\theta_{\text{edge}}|$  reveals that SiftFunnel reduces the edge model’s load by nearly 20 times.

2) *The effect of model architecture.* Changing the model architecture does not affect the parameter settings of the proposed method,

which remain consistent with Section 6.1. We adapt the model to a ResNet-18 with skip connections, using the first residual block as the edge model. This setup is challenging for defense techniques, as shallow networks are simple and do not alter spatial dimensions. Table 3 shows minimal MI impact in unprotected models, leading to weak resistance against MIAs, with MLE-based MIA achieving an MSE of  $10^{-4}$  and Gen-based MIA  $10^{-3}$ . Under these conditions, existing perturbation-based defenses fail to balance usability and privacy effectively, resulting in poor defense performance. Among IB-based defenses, only VIB demonstrates resistance to MLE-based MIA by leveraging the estimation of  $I(x, z)$  as a loss to optimize the edge model. However, its effectiveness remains limited, particularly against Gen-based MIA. For BiDO, despite following the kernel bandwidth estimation methods from [34] and performing extensive experimental tuning, it fails to provide a configuration that balances usability and privacy, ultimately leading to suboptimal defense outcomes. InfoSCISSORS demonstrates some impact on MI under this configuration, but the increase in  $\delta(z)$  undermines its

**Table 6: SiftFunnel Ablation Study on CIFAR-10. The target edge model is the first residual block of ResNet-18, with Gen-based MIA as the attack method. The Red area indicates the strong attack hypothesis from Section 5.2.**

Method	Test ACC $\uparrow$	MSE $\uparrow$	PSNR $\downarrow$	SSIM $\downarrow$	MI $\downarrow$	$\delta(z)$ $\downarrow$
Unprotected	90.43%	0.0010	34.6599	0.9991	0.9719	182,134
Without Funnel (Average training round takes 1 minute, batchsize=64)	<b>90.33% (-0.10%)</b>	0.0594	17.0709	0.7776	0.8945	24,322
Without Attention Blocks	88.45% (-1.98%)	0.0525	17.5709	0.8178	0.8763	<b>3,904</b>
Without KL and LS	88.59% (-1.84%)	0.0850	15.4813	0.6905	0.7935	3,994
Without $\mathcal{L}_{dCor}$	88.77% (-1.66%)	0.0268	20.4929	0.9025	0.9505	4,013
Without $\mathcal{L}_{Pearson}$	88.83% (-1.60%)	0.0492	17.8576	0.8294	0.8618	4,037
Without $l_1$	88.48% (-1.95%)	0.0789	15.8057	0.7272	0.8158	4,030
Attack SiftFunnel in Cloud	88.43% (-2.00%)	0.0521	17.6159	0.8205	0.8905	176,380
SiftFunnel		<b>0.2790</b>	<b>10.3230</b>	<b>0.3001</b>	<b>0.4772</b>	4,028

defense effectiveness against Gen-based MIA, showing only marginal improvements. AE-based defenses exhibit certain resistance to attacks on low-dimensional features in earlier stages, but under the ResNet configuration, their performance diminishes. While this method reduces  $\delta(z)$  by 60%, it has minimal impact on MI, with only a 0.04% decrease. Consequently, AE-based defenses struggle to counter both black-box and gray-box Gen-based MIAs effectively.

In contrast, SiftFunnel reduces MI by 50% and lowers  $\delta(z)$  to the millesimal scale, achieving the best resistance against MIAs while maintaining usability and deployability. Notably, it achieves a minimum SSIM of 0.0793, highlighting its superior performance in balancing privacy and usability.

3) *The effect of data type.* Changes in data types lead to shifts in task requirements. For instance, in this study, the facial recognition task involves 530 classes, while ChestX-ray classification involves 4 classes, necessitating parameter adjustments as shown in Table 5. As analyzed in the previous section on model architectures, to achieve better defense performance, we adjusted the edge model divisions for ResNet-18 and VGG. Specifically, the division points were set after the second residual block for ResNet and after the first ReLU layer following the second max-pooling layer for VGG. The results, summarized in the table 4, show that the defense performance remains unaffected by changes in data types. SiftFunnel continues to be the best defense method, offering an optimal balance between usability, privacy, and deployability.

4) *Ablation Study.* To validate the effectiveness of SiftFunnel’s model structure and loss function design, as well as its defense capability, we conducted ablation experiments using Gen-based MIA. As shown in Table 6, we separately removed the Information Funnel and Attention Blocks from the model structure. The results indicate that removing the Funnel had minimal impact on accuracy, with only a 0.1% decrease, while removing the attention mechanism led to a significant increase in MI compared to SiftFunnel. For the loss function, we evaluated the impact of individually removing KL divergence, linear and nonlinear constraints, and the  $l_1$ -norm. The results demonstrate that KL divergence and  $l_1$ -norm moderately improved defense, whereas nonlinear constraints played a critical role; removing them increased the MSE to 0.0268. Additionally, we

verified the hypothesis from Section 5.2, showing that even when adversaries reconstructed input using features from the cloud’s compensation module, SiftFunnel outperformed existing defenses in protecting transmitted features.

We also evaluated the processing speed of the edge model on both CPU and GPU under this configuration. For single-sample input, the unprotected edge model had a CPU latency of 1.204ms, the AE-based protected model had 2.812ms, and SiftFunnel achieved 2.192ms. On GPU, the processing latency was 3.9ms, 4.3ms, and 6.9ms, respectively. While SiftFunnel showed slightly higher latency on GPU, it required significantly less memory, enabling more parallel processing of inputs under the same resource constraints.

## 7 DISCUSSION

Systematic experiments validated both the criterion and the effectiveness of the method. However, our analysis revealed that achieving optimal resistance against attacks remains challenging for current defense methods, including SiftFunnel, particularly when applied to shallow edge neural networks. When edge models perform only basic feature processing, even SiftFunnel can still allow Gen-based MIA to reconstruct blurred feature structures, while other methods are more vulnerable to input reconstruction. Enhancing privacy protection for extremely shallow edge neural networks presents a promising direction for future research.

Additionally, using MI as an evaluation metric, we observed that some defense methods result in only a 0.5% reduction in MI between inputs and features, yet current MLE-based MIAs still fail to bypass these defenses. This is directly linked to the lack of advancement in existing attack methods. Based on our experimental findings, we suggest that further exploration of more powerful MIAs in white-box scenarios could be a potential research direction.

## 8 CONCLUSION

The increasing complexity of neural networks and inference tasks, alongside the demand for efficiency and real-time feedback, presents significant challenges for edge devices with limited resources. Collaborative inference offers a solution by delegating feature extraction to edge devices and offloading subsequent tasks to the cloud,

but this process leaves transmitted features vulnerable to MIAs. To address these vulnerabilities, we established a first criterion  $D_{mia}$  for evaluating MIA difficulty and proposed SiftFunnel, a privacy-preserving framework designed to limit redundant information and enhance usability. By integrating linear and non-linear correlation constraints, label smoothing, and a funnel-shaped edge model with attention mechanisms, SiftFunnel achieves robust privacy protection while maintaining usability and deployability. Experimental results demonstrate its effectiveness, achieving superior defense against MIAs with minimal accuracy loss and a balanced trade-off among usability, privacy, and practicality.

## REFERENCES

- [1] Martin Abadi, Andy Chu, Ian Goodfellow, H Brendan McMahan, Ilya Mironov, Kunal Talwar, and Li Zhang. 2016. Deep learning with differential privacy. In *Proceedings of the 2016 ACM SIGSAC conference on computer and communications security*. 308–318.
- [2] Kenneth J Arrow. 1969. Classificatory notes on the production and transmission of technological knowledge. *The American Economic Review* 59, 2 (1969), 29–35.
- [3] Bardia Azizian and Ivan V Bajić. 2024. Privacy-Preserving Autoencoder for Collaborative Object Detection. *IEEE Transactions on Image Processing* (2024).
- [4] Mohamed Ishmael Belghazi, Aristide Baratin, Sai Rajeshwar, Sherjil Ozair, Yoshua Bengio, Aaron Courville, and Devon Hjelm. 2018. Mutual information neural estimation. In *International conference on machine learning*. PMLR, 531–540.
- [5] Pengyu Cheng, Weituo Hao, Shuyang Dai, Jiachang Liu, Zhe Gan, and Lawrence Carin. 2020. Club: A contrastive log-ratio upper bound of mutual information. In *International conference on machine learning*. PMLR, 1779–1788.
- [6] Israel Cohen, Yiteng Huang, Jingdong Chen, Jacob Benesty, Jacob Benesty, Jingdong Chen, Yiteng Huang, and Israel Cohen. 2009. Pearson correlation coefficient. *Noise reduction in speech processing* (2009), 1–4.
- [7] Sayanton V Dibbo. 2023. Sok: Model inversion attack landscape: Taxonomy, challenges, and future roadmap. In *2023 IEEE 36th Computer Security Foundations Symposium (CSF)*. IEEE, 439–456.
- [8] Shiwei Ding, Lan Zhang, Miao Pan, and Xiaoyong Yuan. 2024. PATROL: Privacy-Oriented Pruning for Collaborative Inference Against Model Inversion Attacks. In *Proceedings of the IEEE/CVF Winter Conference on Applications of Computer Vision*. 4716–4725.
- [9] Monroe D Donsker and SR Srinivasa Varadhan. 1983. Asymptotic evaluation of certain Markov process expectations for large time. IV. *Communications on pure and applied mathematics* 36, 2 (1983), 183–212.
- [10] Lin Duan, Jingwei Sun, Yiran Chen, and Maria Gorlatova. 2023. PrivaScissors: Enhance the Privacy of Collaborative Inference through the Lens of Mutual Information. *arXiv preprint arXiv:2306.07973* (2023).
- [11] Apple Security Engineering and Architecture. 2024. *Private Cloud Compute: A new frontier for AI privacy in the cloud*.
- [12] Matt Fredrikson, Somesh Jha, and Thomas Ristenpart. 2015. Model inversion attacks that exploit confidence information and basic countermeasures. In *Proceedings of the 22nd ACM SIGSAC conference on computer and communications security*. 1322–1333.
- [13] Matthew Fredrikson, Eric Lantz, Somesh Jha, Simon Lin, David Page, and Thomas Ristenpart. 2014. Privacy in pharmacogenetics: An {End-to-End} case study of personalized warfarin dosing. In *23rd USENIX security symposium (USENIX Security 14)*. 17–32.
- [14] Lovedeep Gondara. 2016. Medical image denoising using convolutional denoising autoencoders. In *2016 IEEE 16th international conference on data mining workshops (ICDMW)*. IEEE, 241–246.
- [15] Arthur Gretton, Olivier Bousquet, Alex Smola, and Bernhard Schölkopf. 2005. Measuring statistical dependence with Hilbert-Schmidt norms. In *International conference on algorithmic learning theory*. Springer, 63–77.
- [16] Arthur Gretton, Ralf Herbrich, Alexander Smola, Olivier Bousquet, Bernhard Schölkopf, and Aapo Hyvärinen. 2005. Kernel methods for measuring independence. *Journal of Machine Learning Research* 6, 12 (2005).
- [17] Koh Jun Hao, Sy-Tuyen Ho, Ngoc-Bao Nguyen, and Ngai-Man Cheung. 2025. On the Vulnerability of Skip Connections to Model Inversion Attacks. In *European Conference on Computer Vision*. Springer, 140–157.
- [18] Kaiming He, Xiangyu Zhang, Shaoqing Ren, and Jian Sun. 2016. Deep residual learning for image recognition. In *Proceedings of the IEEE conference on computer vision and pattern recognition*. 770–778.
- [19] Zecheng He, Tianwei Zhang, and Ruby B Lee. 2019. Model inversion attacks against collaborative inference. In *Proceedings of the 35th Annual Computer Security Applications Conference*. 148–162.
- [20] Zecheng He, Tianwei Zhang, and Ruby B Lee. 2020. Attacking and protecting data privacy in edge-cloud collaborative inference systems. *IEEE Internet of Things Journal* 8, 12 (2020), 9706–9716.
- [21] Sy-Tuyen Ho, Koh Jun Hao, Keshigeyan Chandrasegaran, Ngoc-Bao Nguyen, and Ngai-Man Cheung. 2024. Model Inversion Robustness: Can Transfer Learning Help?. In *Proceedings of the IEEE/CVF Conference on Computer Vision and Pattern Recognition*. 12183–12193.
- [22] Fanliang Hu, Jian Shen, and Pandi Vijayakumar. 2023. Side-Channel Attacks Based on Multi-Loss Regularized Denoising AutoEncoder. *IEEE Transactions on Information Forensics and Security* (2023).
- [23] Jie Hu, Li Shen, and Gang Sun. 2018. Squeeze-and-excitation networks. In *Proceedings of the IEEE conference on computer vision and pattern recognition*. 7132–7141.
- [24] Jacob Huckelberry, Yuke Zhang, Allison Sansone, James Mickens, Peter A Beerel, and Vijay Janapa Reddi. 2024. TinyML Security: Exploring Vulnerabilities in Resource-Constrained Machine Learning Systems. *arXiv preprint arXiv:2411.07114* (2024).
- [25] Shuaifan Jin, He Wang, Zhibo Wang, Feng Xiao, Jiahui Hu, Yuan He, Wenwen Zhang, Zhongjie Ba, Weijie Fang, Shuhong Yuan, et al. 2024. {FaceObfuscator}: Defending Deep Learning-based Privacy Attacks with Gradient Descent-resistant Features in Face Recognition. In *33rd USENIX Security Symposium (USENIX Security 24)*. 6849–6866.
- [26] Alex Krizhevsky, Geoffrey Hinton, et al. 2009. Learning multiple layers of features from tiny images. (2009).
- [27] Runze Li, Wei Zhong, and Liping Zhu. 2012. Feature screening via distance correlation learning. *J. Amer. Statist. Assoc.* 107, 499 (2012), 1129–1139.
- [28] Rongke Liu, Dong Wang, Yizhi Ren, Zhen Wang, Kaitian Guo, Qianqian Qin, and Xiaolei Liu. 2024. Unstoppable Attack: Label-Only Model Inversion via Conditional Diffusion Model. *IEEE Transactions on Information Forensics and Security* (2024).
- [29] Ziwei Liu, Ping Luo, Xiaogang Wang, and Xiaoou Tang. 2015. Deep learning face attributes in the wild. In *Proceedings of the IEEE international conference on computer vision*. 3730–3738.
- [30] Shaguftha Mehnaz, Sayanton V Dibbo, Roberta De Viti, Ehsanul Kabir, Björn B Brandenburg, Stefan Mangard, Ninghui Li, Elisa Bertino, Michael Backes, Emiliano De Cristofaro, et al. 2022. Are your sensitive attributes private? novel model inversion attribute inference attacks on classification models. In *31st USENIX Security Symposium (USENIX Security 22)*. 4579–4596.
- [31] Fatemehsadat Miresghallah, Mohammadkazem Taram, Ali Jalali, Ahmed Taha Taha Elthakeb, Dean Tullsen, and Hadi Esmaeilzadeh. 2021. Not all features are equal: Discovering essential features for preserving prediction privacy. In *Proceedings of the Web Conference 2021*. 669–680.
- [32] Diganta Misra, Trikey Nalamada, Ajay Uppili Arasanipalai, and Qibin Hou. 2021. Rotate to Attend: Convolutional Triplet Attention Module. In *2021 IEEE Winter Conference on Applications of Computer Vision (WACV)*. 3138–3147. <https://doi.org/10.1109/WACV48630.2021.00318>
- [33] Hong-Wei Ng and Stefan Winkler. 2014. A data-driven approach to cleaning large face datasets. In *2014 IEEE international conference on image processing (ICIP)*. IEEE, 343–347.
- [34] Xiong Peng, Feng Liu, Jingfeng Zhang, Long Lan, Junjie Ye, Tongliang Liu, and Bo Han. 2022. Bilateral dependency optimization: Defending against model-inversion attacks. In *Proceedings of the 28th ACM SIGKDD Conference on Knowledge Discovery and Data Mining*. 1358–1367.
- [35] Yuben Qu, Hao Sun, Chao Dong, Jiawen Kang, Haipeng Dai, Qihui Wu, and Song Guo. 2023. Elastic collaborative edge intelligence for UAV swarm: Architecture, challenges, and opportunities. *IEEE Communications Magazine* (2023).
- [36] Jorma J Rissanen. 1996. Fisher information and stochastic complexity. *IEEE transactions on information theory* 42, 1 (1996), 40–47.
- [37] Leonid I Rudin, Stanley Osher, and Emad Fatemi. 1992. Nonlinear total variation based noise removal algorithms. *Physica D: nonlinear phenomena* 60, 1-4 (1992), 259–268.
- [38] Unais Sait, K Lal, S Prajapati, Rahul Bhaumik, Tarun Kumar, S Sanjana, and Kriti Bhalla. 2020. Curated dataset for covid-19 posterior-anterior chest radiography images (x-rays). *Mendeley Data* 1, J (2020).
- [39] Nir Shlezinger and Ivan V Bajić. 2022. Collaborative inference for AI-empowered IoT devices. *IEEE Internet of Things Magazine* 5, 4 (2022), 92–98.
- [40] Nir Shlezinger, Erez Farhan, Hai Morgenstern, and Yonina C Eldar. 2021. Collaborative inference via ensembles on the edge. In *ICASSP 2021-2021 IEEE International Conference on Acoustics, Speech and Signal Processing (ICASSP)*. IEEE, 8478–8482.
- [41] Karen Simonyan. 2014. Very deep convolutional networks for large-scale image recognition. *arXiv preprint arXiv:1409.1556* (2014).
- [42] Lukas Struppek, Dominik Hintersdorf, Antonio De Almeida Correia, Antonia Adler, and Kristian Kersting. 2022. Plug & play attacks: Towards robust and flexible model inversion attacks. *arXiv preprint arXiv:2201.12179* (2022).
- [43] Lukas Struppek, Dominik Hintersdorf, and Kristian Kersting. 2023. Be careful what you smooth for: Label smoothing can be a privacy shield but also a catalyst for model inversion attacks. *arXiv preprint arXiv:2310.06549* (2023).
- [44] Christian Szegedy, Sergey Ioffe, Vincent Vanhoucke, and Alexander Alemi. 2017. Inception-v4, inception-resnet and the impact of residual connections on learning. In *Proceedings of the AAAI conference on artificial intelligence*, Vol. 31.

- [45] Tianhao Wang, Yuheng Zhang, and Ruoxi Jia. 2021. Improving robustness to model inversion attacks via mutual information regularization. In *Proceedings of the AAAI Conference on Artificial Intelligence*, Vol. 35. 11666–11673.
- [46] Yulong Wang, Xingshu Chen, and Qixu Wang. 2022. Privacy-preserving Security Inference Towards Cloud-Edge Collaborative Using Differential Privacy. *arXiv preprint arXiv:2212.06428* (2022).
- [47] Yanhu Wang, Shuaishuai Guo, Yiqin Deng, Haixia Zhang, and Yuguang Fang. 2024. Privacy-preserving task-oriented semantic communications against model inversion attacks. *IEEE Transactions on Wireless Communications* (2024).
- [48] Sanghyun Woo, Jongchan Park, Joon-Young Lee, and In So Kweon. 2018. Cbam: Convolutional block attention module. In *Proceedings of the European conference on computer vision (ECCV)*. 3–19.
- [49] Yixiao Xu, Binxing Fang, Mohan Li, Xiaolei Liu, and Zhihong Tian. 2024. Query-Efficient Model Inversion Attacks: An Information Flow View. *IEEE Transactions on Information Forensics and Security* (2024).
- [50] Mengda Yang, Ziang Li, Juan Wang, Hongxin Hu, Ao Ren, Xiaoyang Xu, and Wenzhe Yi. 2022. Measuring data reconstruction defenses in collaborative inference systems. *Advances in Neural Information Processing Systems* 35 (2022), 12855–12867.
- [51] Ziqi Yang, Jiyi Zhang, Ee-Chien Chang, and Zhenkai Liang. 2019. Neural network inversion in adversarial setting via background knowledge alignment. In *Proceedings of the 2019 ACM SIGSAC Conference on Computer and Communications Security*. 225–240.
- [52] Yupeng Yin, Xianglong Zhang, Huanle Zhang, Feng Li, Yue Yu, Xiuzhen Cheng, and Pengfei Hu. 2023. Ginver: Generative model inversion attacks against collaborative inference. In *Proceedings of the ACM Web Conference 2023*. 2122–2131.
- [53] Xiaojian Yuan, Kejiang Chen, Jie Zhang, Weiming Zhang, Nenghai Yu, and Yang Zhang. 2023. Pseudo label-guided model inversion attack via conditional generative adversarial network. In *Proceedings of the AAAI Conference on Artificial Intelligence*, Vol. 37. 3349–3357.
- [54] Huan Zhang, Hongge Chen, Zhao Song, Duane Boning, Inderjit S Dhillon, and Cho-Jui Hsieh. 2019. The limitations of adversarial training and the blind-spot attack. *arXiv preprint arXiv:1901.04684* (2019).
- [55] Ruisi Zhang, Seira Hidano, and Farinaz Koushanfar. 2022. Text revealer: Private text reconstruction via model inversion attacks against transformers. *arXiv preprint arXiv:2209.10505* (2022).
- [56] Yuheng Zhang, Ruoxi Jia, Hengzhi Pei, Wenxiao Wang, Bo Li, and Dawn Song. 2020. The secret revealer: Generative model-inversion attacks against deep neural networks. In *Proceedings of the IEEE/CVF conference on computer vision and pattern recognition*. 253–261.
- [57] Zeping Zhang, Xiaowen Wang, Jie Huang, and Shuaishuai Zhang. 2023. Analysis and Utilization of Hidden Information in Model Inversion Attacks. *IEEE Transactions on Information Forensics and Security* (2023).
- [58] Xiaochen Zhu, Xinjian Luo, Yuncheng Wu, Yangfan Jiang, Xiaokui Xiao, and Beng Chin Ooi. 2023. Passive Inference Attacks on Split Learning via Adversarial Regularization. *arXiv preprint arXiv:2310.10483* (2023).